



## Paclitaxel-loaded multifunctional nanoparticles for the targeted treatment of glioblastoma

Lakshmi Pallavi Ganipineni, Bernard Ucakar, Nicolas Joudiou, Raphaël Riva, Christine Jérôme, Bernard Gallez, Fabienne Danhier & Véronique Prétat

To cite this article: Lakshmi Pallavi Ganipineni, Bernard Ucakar, Nicolas Joudiou, Raphaël Riva, Christine Jérôme, Bernard Gallez, Fabienne Danhier & Véronique Prétat (2019): Paclitaxel-loaded multifunctional nanoparticles for the targeted treatment of glioblastoma, Journal of Drug Targeting, DOI: [10.1080/1061186X.2019.1567738](https://doi.org/10.1080/1061186X.2019.1567738)

To link to this article: <https://doi.org/10.1080/1061186X.2019.1567738>



Accepted author version posted online: 11 Jan 2019.



Submit your article to this journal [↗](#)



Article views: 1



View Crossmark data [↗](#)

## **Paclitaxel-loaded multifunctional nanoparticles for the targeted treatment of glioblastoma**

Lakshmi Pallavi Ganipineni<sup>1</sup>, Bernard Ucakar<sup>1</sup>, Nicolas Joudiou<sup>2</sup>, Raphaël Riva<sup>3</sup>, Christine Jérôme<sup>3</sup>, Bernard Gallez<sup>2</sup>, Fabienne Danhier<sup>1</sup>, Véronique Prémat<sup>1\*</sup>

<sup>1</sup> Université Catholique de Louvain, Advanced Drug Delivery and Biomaterials, Louvain Drug Research Institute, Brussels, Belgium

<sup>2</sup> Université Catholique de Louvain, Nuclear and Electron Spin Technologies Platform (NEST), Louvain Drug Research Institute, Brussels, Belgium

<sup>3</sup> University of Liège, Center for Education and Research on Macromolecules (CERM), CESAM Research Unit, Liège, Belgium

\* Correspondence: Prof. Véronique Prémat

Université Catholique de Louvain

LDRI–Avenue Mounier 73, Boîte b1.7312, 1200 Brussels – Belgium

Tel: + 32 2 764 73 09

Fax: + 32 2 764 73 98

Email: veronique.preat@uclouvain.be

**Abstract:** We hypothesized that the active targeting of  $\alpha v\beta 3$  integrin overexpressed in neoangiogenic blood vessels and glioblastoma (GBM) cells combined with magnetic targeting of paclitaxel- and SPIO-loaded PLGA-based nanoparticles could improve accumulation of nanoparticles in the tumor and therefore improve the treatment of GBM.

Methods: PTX/SPIO PLGA nanoparticles with or without RGD-grafting were characterized. Their *in vitro* cellular uptake and cytotoxicity was evaluated by fluorospectroscopy and MTT assay. *In vivo* safety and anti-tumor efficacy of different targeting strategies was evaluated in orthotopic U87MG tumor model over multiple intravenous injections.

Results: The nanoparticles of 250nm were negatively charged. RGD targeted nanoparticles showed a specific and higher cellular uptake than untargeted nanoparticles by activated U87MG and HUVEC cells. *In vitro* IC<sub>50</sub> of PTX after 48h was approximately 1 ng/mL for all the PTX-loaded nanoparticles. The median survival time of the mice treated with magnetic targeted nanoparticles was higher than the control (saline) mice or mice treated with other evaluated strategies. The 6 doses of PTX did not induce any detectable toxic effects on liver, kidney and heart when compared to Taxol.

Conclusion. The magnetic targeting strategy resulted in better therapeutic effect than the other targeting strategies (passive, active).

**Key words:** PLGA nanoparticles, Glioblastoma, Targeting, Nanomedicine, nanotheranostics, Paclitaxel.

## Introduction

Glioblastoma (GBM) is one of the most prevalent and deadliest malignant tumors that occur in central nervous system [1, 2]. GBM is featured with rapid proliferation, high invasiveness, extensive infiltration, hyper neoangiogenesis and is very challenging to treat with the current therapies [2]. Advances in drug discovery and therapeutic payload delivery, did not significantly improve the survival rates of GBM patients which has remained at an average of less than 18 months [3]. The current standard care for GBM includes maximal safe resection, followed by radiotherapy and concomitant treatment with alkylating agents. However, the standard treatments face limitations such as practically impossible complete resection of tumor, high recurrence rate and overall resistance to therapy [3]. Due to the current survival expectancy and the existing limitations of the available treatments, there is a great need for better and promising therapies for devastating GBM.

The versatility and ability of nanoscale systems as efficient drug targeting and delivery systems for GBM have been previously demonstrated. Nanomedicine has the ability to address some of critical limitations of the conventional drugs such as inability to cross the biological barriers, poor accumulation at the targeted brain tumor site and high systemic side effects [4, 5, 6].

Poly(lactic-*co*-glycolic acid) (PLGA) is one of the most widely used biocompatible and biodegradable polymers for preparation of nanoparticles (NPs). It is approved by regulatory agencies for parenteral products [7]. PLGA allows encapsulation of potential chemotherapeutic drugs, which face solubility difficulties in conventional forms. Polyethylene glycol (PEG) hydrophilic stabilizing sheath around the hydrophobic core of PLGA protect the NPs from the RES clearance [7]. Encapsulation of anticancer drugs in PLGA has been exploited to ameliorate drug delivery in cancer, including GBM [8, 9].

Paclitaxel (PTX) is a microtubule stabilizing, potent anti-neoplastic agent used as first line therapy against many tumors such as small cell lung carcinoma, breast cancer [10]. Even though PTX is a highly potent agent, its use in clinical treatment for GBM is limited because of its failure to reach the brain. It has been reported that PTX encapsulated in nanocarriers can cross a disrupted or leaky blood brain barrier (BBB), exerts a therapeutic effect in preclinical GBM models and lower side effects [11, 12, 13, 14].

In addition, a suitable targeting strategy can add more value to the whole formulation and increase therapeutic efficacy. Given the selectivity problem of most of the anti-cancer drugs, various efforts

are being put forth for specific targeting of tumor cells [15]. Different targeting strategies have been explored. The benefit of nanomedicine can partly be attributed to so called passive targeting i.e., the accumulation of NPs *via* the controversial enhanced permeability and retention (EPR) effect, which is a result of leaky vasculature and/or poor lymphatic drainage system of tumor [16, 17]. Active targeting takes advantage of specific moieties expressed on the surface of cancer cells or tumor microenvironment. Specific targeting ligands functionalized on the surface of NPs that have affinity to interact or bind to those moieties can enhance drug amount and/or intracellular uptake of NPs (active targeting) [17]. GBM cells are infiltrative in nature as a consequence of expression of integrin that facilitates migration and infiltration into surrounding healthy brain tissue [18]. The expression of  $\alpha\beta3$  integrin (a class of cell adhesion receptors) is prominent in GBM biopsy samples at both tumor microvessels and tumor cells [19]. Overexpression of  $\alpha\beta3$  integrin is more dominant in highly proliferating and infiltrating areas of GBM [19]. This overexpression can make RGD (tripeptide)-based targeting an effective strategy for drug delivery to GBM tumors as the short peptide sequence is specific and well recognized by  $\alpha\beta3$  integrins [12, 13, 20, 21].

Application of external stimuli could also increase the accumulation of NPs into the desired tissues. In particular, application of an external magnetic field can attract magnetic NPs by magnetic targeting [22]. Superparamagnetic iron oxide nanoparticles (SPIOs) were used for imaging as a  $T_2$  contrast agent for magnetic resonance imaging (MRI) and magnetic targeting purposes [23, 24, 25, 26]. SPIONs when used in a hybrid targeting strategy (active and/or magnetic) further topped-up the passive accumulation of NPs leading to improved therapeutic efficacy in a colorectal tumor [27].

We have previously shown that magnetic targeting alone induced significant increase in accumulation of PTX and SPIO loaded PLGA-based NPs at tumor site and prolonged the survival period in orthotopic glioma tumor model [14]. In our current study, we hypothesized that active targeting of  $\alpha\beta3$  integrin which is overexpressed in neoangiogenic blood vessels and GBM cells combined with magnetic targeting of PTX-loaded PLGA NPs would improve the treatment of orthotopic GBM model by further enhancing accumulation in the tumor and/or by increasing the endocytosis of the NPs. For this, we have evaluated in an orthotopic U87MG tumor model different targeting strategies: passive targeting by EPR effect as control for other targeting strategies, active targeting *via* RGD targeting of  $\alpha\beta3$  integrin, magnetic targeting of SPIO-loaded formulation and active combined with magnetic targeting.

## Material and methods

### 2.1 Materials

Ring-opening polymerization method was used to synthesize PCL-*b*-PEG (13100–5000); PLGA-*b*-PEG (10040–4600), and fluorescein isothiocyanate (FITC)-PLGA (23,600) as previously described [28, 29, 30]. PLGA (50:50 lactide/glycolide; 7000 to 17000), sodium hydroxide, iron(III) chloride, iron(II) chloride, oleic acid, hydrochloric acid, MTT (3-(4,5-dimethylthiazol-2-yl)-2,5-diphenyltetrazolium bromide)) PVA (polyvinyl alcohol; 30–70 kDa), GRGDS peptide (linear), anti-human IgG, Human umbilical vein endothelial cells (HUVEC) (200P-05N), Endothelial Cell Growth Medium and xylozine hydrochloride were bought from Sigma-Aldrich (USA). TPD clip 4-[3-(trifluoromethyl)diazirin-3-yl]benzoic acid *n*-hydroxysuccinimide ester was obtained from Toronto research chemicals (Canada) and monoclonal anti-human integrin-  $\alpha\beta 3$  (CD51/61)-phycoerythrin antibody from R&D systems (USA). Poly-D-Lysine hydrobromide (70000 to 150000) was bought from MP Biomedicals (Germany). Trypsin EDTA, penicillin-streptomycin, Fetal bovine serum (FBS) and Eagle's Minimum Essential Medium were obtained from Gibco<sup>®</sup> BRL (USA). Ketamine (100mg/mL; Nimatek) from Eurovet Animal Health B.V. (The Netherlands). U87MG cells (HTB-14<sup>™</sup>), were obtained from ATCC. Formaldehyde (4% solution) was bought from Merck (Germany). Analytical grade solvents and chemicals were used for all the experiments.

### 2.2 Formulation and physicochemical characterization

#### 2.2.1 Photografting of RGD to PCL-*b*-PEG copolymer

RGD was grafted to PCL-*b*-PEG copolymer as described by Pourcelle et al [31]. Briefly, PCL-*b*-PEG was dissolved in acetonitrile with TPD clip (molecular clip). The solution was cast on glass plates and then subjected to evaporation followed by vacuum drying until constant weight. Fully dried copolymer was collected and irradiated in a homemade reactor [3 UV lamps (8 watts for each lamp) placed at a distance of 4.5 cm from rotating quartz flask] at 254 nm under inert atmosphere for 90 min. The clip grafted copolymer (activated copolymer) was then washed with isopropanol:ethyl acetate (19:1) and dried under vacuum before being mixed with GRGDS peptide 1 mM solution. After 24 h of shaking at room temperature, the RGD grafted polymer was washed 3 times with 5 mM HCl, 5 times with deionized water and vacuum dried. As the molecular clip

contain F,  $^{19}\text{F}$  NMR was used to demonstrate the activation of molecular clip, which is crucial step for the successful grafting of RGD onto NHS ester [31] (see supplementary data S1).

### *2.2.2 Preparation and physicochemical characterization of RGD functionalized PTX and SPIO-loaded nanoparticles (PTX/SPIO-RGD-NPs)*

SPIO coated with oleic acid were synthesized as previously described [32] by coprecipitation method using ferrous and ferric salts in an alkaline medium under argon atmosphere and at  $80^\circ$ .

PTX/SPIO-NPs were prepared by an emulsion–diffusion–evaporation method with a few modifications [33]. Initially, PTX (2.5 mg), PLGA (70 mg), PCL-b-PEG (15 mg) and PLGA-b-PEG (15 mg) in dichloromethane were added with SPIO (7.7 mg/mL iron [Fe] concentration) and mixed well. Secondly, 3% PVA aqueous solution was added to the mixture, vortexed and emulsified at 50 W using an ultrasonicator ( $3 \times 30$  s) resulting in an emulsion. Thirdly, the resulted emulsion was added dropwise to a 1% PVA aqueous solution under magnetic stirring at 400 rpm and left for organic solvent evaporation. Then the NPs were washed with water. Finally, the NPs were suspended in 1mL of water. Same procedures were followed to prepare SPIO-NPs, FITC labelled PLGA NPs and PTX-loaded NPs (PTX-NPs). Similarly, PTX/SPIO-RGD-NPs and FITC labelled PLGA RGD NPs were prepared using RGD grafted PCL-PEG.

PLGA-based NPs loaded with PTX and SPIO (PTX/SPIO-NPs), PTX-NPs, SPIO, SPIO-NPs and FITC labelled PLGA NPs were formulated and characterized for size (dynamic light scattering), zeta potential (laser Doppler velocimetry) using NanoSizer Zeta Series instrument (Malvern, UK). Encapsulation efficiency [percent ratio of entrapped drug (mg) to total drug (mg)] and drug loading [percent ratio of entrapped drug (mg) to 100 mg polymer] of PTX were measured using by high-performance liquid chromatography with ultraviolet detection at 227 nm (Agilent 1100 series instrument; Agilent Technologies). Iron loading was determined by electron spin resonance (ESR) spectroscopy (Bruker Optik GmbH, Germany) and validated by inductively coupled plasma mass spectrometry (ICP-MS) using an Agilent 7500ce instrument (Agilent Technologies, CA, USA) as previously reported [14, 33].

## **2.3 In vitro studies**

### *2.3.1 Cellular uptake of PTX/SPIO-NPs versus PTX/SPIO-RGD-NPs*

U87MG cells expression of  $\alpha\text{v}\beta3$  was evaluated by flow cytometry using monoclonal anti-human integrin-  $\alpha\text{v}\beta3$  (CD51/61)-phycoerythrin antibody, adapted from [34]. U87MG cells ( $5 \times 10^4$ ) were

incubated with anti-human IgG (1  $\mu\text{g}$ ; 15 min) to block non-specific binding. The cells were incubated with anti-human integrin- $\alpha\beta 3$  (CD51/61)-phycoerythrin monoclonal antibody (0.05  $\mu\text{g}$ ; 4°C for 60 min), washed with PBS, trypsinized (0.05%) and analyzed by flow cytometer (FACScan, Becton Dickinson) The cells incubated without monoclonal antibody was used as control.

The cellular uptake of NPs was evaluated in U87MG cells (passage 10) and in HUVEC (passage 3) [35]. HUVEC cells were seeded ( $2 \times 10^4$ ) in 48-well culture plates coated with 0.2% gelatin. U87MG cells were seeded ( $4 \times 10^4$ ) in 24-well culture plates. After 24 h incubation, the cells were activated with TNF- $\alpha$  (10ng/mL; to enhance  $\alpha\beta 3$  integrin expression) followed by treatment with 0.1% BSA (to inhibit non-specific binding). Then the cells were incubated with FITC-NPs and FITC-RGD-NPs (10 mg/ml polymer concentration) at 37 °C for 4 h. The cells were rinsed with PBS and detached with trypsin (0.05%). A competition assay was performed on activated cells by incubating with excess of GRGDS peptide for 30 min followed by incubating with NPs for 4 h. The fluorescent NPs uptake was quantified by measuring fluorescence intensity using Packard Fluorocount Microplate fluometer (Packard Instrument Company, Meriden, CT, USA) at 485/530 nm excitation/emission wavelengths.

### 2.3.2 Cellular cytotoxicity

The cytotoxicity of PTX-NPs, SPIO-NPs and PTX/SPIO-NPs was determined by a MTT cell proliferation assay [36]. U87MG cells were cultured in EMEM culture medium supplemented with 10% FBS, 100 U/mL penicillin G sodium and 100  $\mu\text{g}/\text{mL}$  streptomycin sulfate. For MTT assay, cells were seeded at a density of  $5 \times 10^3$  cells per well in 96-well plates and after 24 h different formulations (PTX-NPs, SPIO-NPs and PTX/SPIO-NPs, PTX/SPIO-RGD-NPs) at different PTX concentrations [0.01 ng/ml - 10000 ng/ml PTX (~100  $\mu\text{g}/\text{mL}$  of polymer concentration)] were added to the cells. Post 48 h, cells were washed with PBS and incubated with the medium containing MTT (5 mg/ml) for an additional 4 h. Then MTT solution was removed and DMSO was added. Absorbance of treated and untreated cells was measured (BioRad microplate reader, USA) at 570 nm. The results are presented as relative percentage of living cell survival compared to the untreated cells (negative control). IC50 values were calculated using Graph pad prism software.

## 2.4 *In vivo* studies

All experiments were compliant with Belgian national regulation guidelines and approved by the animal care ethical committee of the Université catholique de Louvain (2014/UCL/MD/004).

### 2.4.1 *Orthotopic U87MG tumor model*

NMRI-nude mice (female, 6 weeks old; Janvier, France) were procured followed by 1-week acclimatization. Mice were anaesthetized (intraperitoneal injection of xylazine (13 mg/kg) and ketamine (100 mg/kg)) and were positioned into a stereotaxic frame. For tumor inoculation, a 3  $\mu$ L intracranial injection of U87MG cells in culture medium ( $3 \times 10^4$  cells) was performed into the right frontal lobe (striatum; coordinates: 2.1 mm lateral from bregma, 0.5 mm anterior and 3 mm deep from the outer border of the cranium) using a 5  $\mu$ L Hamilton<sup>®</sup> syringe fitted with a 26G needle.

### 2.4.2 *MRI imaging*

MRI was performed using an 11.7 T Biospec small-animal MR scanner (Bruker BioSpin GmbH Rheinstetten, Germany) to obtain tumor location and volume. Mice were anesthetized using isoflurane (2.5 for induction and 1% for maintenance). Animal respiration was monitored during all the experiment and core temperature was maintained using hot water circulation in a blanket. To monitor the tumor growth anatomical images were obtained using T<sub>2</sub>-weighted rapid acquisition with refocused echoes sequence [RARE]. Parameters were as following: number of averages = 8, matrix size = 200 x 200, field of view [FOV] = 2 x 2 cm, repetition time [TR] = 2500 ms, effective echo time [TE<sub>eff</sub>] = 30 ms, number of continuous slices = 25, slice thickness = 0.3 mm, in-plane resolution = 100  $\mu$ m<sup>2</sup>. Tumor volume was determined from manually drawn region of interest (ROI) using Paravision 6.1 software (Bruker BioSpin), on day 7 and day 28.

### 2.4.3. *In vivo anti-tumor efficacy*

The anti-tumor efficacy of the formulated NPs was evaluated in the orthotopic U87MG tumor model. Mice bearing tumors were assigned uniformly into groups ( $n \geq 5$ ). Dosing regimen was adapted based on previously established protocols [37, 38]. All the groups except the untreated/control (saline) group received six intravenous injections (5 mg/kg PTX and 14 mg/kg Fe; 150  $\mu$ L) over three weeks (supplementary data S2). The experimental endpoint was determined as 20% weight loss or 10% weight loss with tumor related sickness (moribund mouse or mouse lacking complete mobility).

Group 1: Injection of PBS

Group 2: injection of PTX/SPIO-NPs (passive targeting)

Group 3: PTX/SPIO-NPs injection with post application of 1.4 T neodymium magnet for 4 h (magnetic targeting)

Group 4: injection of PTX/SPIO-RGD-NPs (active targeting).

Group 5: Injection of PTX/SPIO-RGD-NPs with application of 1.4 T neodymium magnet for 4 h (magnetic + active targeting).

#### *2.4.4 In vivo safety evaluation*

Mice (Swiss mice; Janvier) were randomly assigned into three groups ( $n=6$ ) and each group received six intravenous injections of PTX/SPIO-NPs (5 mg/kg PTX), Taxol<sup>®</sup> (5 mg/kg PTX) or control (saline) over 3 weeks. Daily monitoring of body weight and collection of blood and tissue samples (at 24 h and 7 days) were performed. Aspartate aminotransferase (AST), alanine aminotransferase (ALT), blood urea nitrogen (BUN) and creatine kinase (isoenzymes CKM and CKB; CKMB) levels were assayed using a Fujifilm DRI-CHEM NX500i Analyzer (Fujifilm, Tokyo, Japan). Hematoxylin and Eosin staining was performed for histological analysis on liver tissue [14].

#### *2.5 Statistical analyses*

All the results were presented as the mean  $\pm$  standard deviation (SD). One-way ANOVA with Tukey post-tests, Two way ANOVA with Bonferroni post-test and Kaplan-Meier survival rate curves were performed using the software Graph Pad Prism 5 for Windows (GraphPad Software, San Diego, USA) to demonstrate significant differences among treatment groups ( $*p < 0.05$ ,  $**p < 0.01$ ,  $***p < 0.001$ ).

### **3. Results**

#### *3.1 Physicochemical properties of PTX and SPIO-loaded nanoparticles*

The formulated NPs were characterized for size, zeta potential, encapsulation efficiency, drug and iron loading as applicable and are summarized in table 1. The PTX-NPs, SPIO-NPs, PTX/SPIO-NPs and PTX/SPIO-RGD-NPs were in size range of approximately 230-255 nm and PDI was  $\leq 0.2$ . All the NPs were negatively charged (less than -15mV). The PTX encapsulation efficiency was  $\sim 30\%$  and drug loading was  $\sim 0.8\%$ . The iron loading was found to be approximately 3%. The TEM images and superparamagnetic properties of the prepared NPs have already been published by our

group [33]. Consistent with our previous reports [27], inclusion of ligand (RGD) grafted copolymer did not alter the size or other physicochemical characters.

### **3.2 *In vitro* cellular uptake studies**

The purpose of *in vitro* cellular uptake studies was to evaluate the effect of RGD on cellular internalization of NPs in U87MG and HUVEC cell lines (Fig. 1). Expression of  $\alpha\beta3$  integrin by U87MG cells was verified before quantitative analysis of the cellular uptake of PLGA-FITC-based fluorescent NP.

The flow-cytometry analysis confirmed that the used U87MG cells expressed  $\alpha\beta3$  (supplementary data S3) in compliance with literature [34]. HUVEC cells activated by TNF- $\alpha$  [39] served as positive control for  $\alpha\beta3$  integrin expression. Both cell lines showed increased uptake of FITC-RGD-NPs ( $p < 0.001$ ) after activation by TNF- $\alpha$  whereas there was no significant change in case of FITC-NPs uptake. HUVEC cells displayed two-fold higher uptake of FITC-RGD-NPs ( $p < 0.001$ ). Competition assay with excess concentration of GRGDS peptide or anti- $\alpha\beta3$  integrin inhibited the enhanced uptake of RGD-NPs by both HUVEC and U87MG cells. This confirms that RGD enhanced the cellular uptake through its favored binding to  $\alpha\beta3$  receptor [35].

### **3.3 *In vitro* cytotoxicity studies**

*In vitro* cytotoxicity of NPs was performed on U87MG cell line (Fig. 2). At the concentration of 0.01 ng/mL, no significant cytotoxic effect was observed. With increasing concentrations of NPs, cell viability significantly decreased except in case of SPIO-NPs, confirming that the cytotoxic effect of the formulation was mainly due to PTX. After 48 h, the IC<sub>50</sub> values of PTX were approximately 1 ng/mL whatever the NPs (0.9 ng/mL for PTX-NPs, 0.8 ng/mL for PTX/SPIO-NPs and 0.9 ng/mL for PTX/SPIO-RGD-NPs), indicating that, inclusion of RGD-grafted PCL-PEG into the formulation did not enhance cytotoxicity effects of PTX/SPIO-NPs.

### **3.4 Noninvasive MRI imaging**

The BBB disruption of U87MG orthotopic tumor model was previously demonstrated [14]. On day 8, the MRI images were obtained before and 4 hours after the first treatment injection (Fig. 3). Repositioning of the animals into MRI was required between the pre- and post-treatment scans due to the application of magnetic targeting. We observed that the contrast difference at the tumor site was visually prominent in groups of active+magnetic group and magnetic group indirectly

indicating accumulation of higher amounts of NPs in comparison to the other groups ( $n \geq 3$ ). There was no difference in the pre and post treatment images of the control (saline) group. Further, we plan to evaluate quantitatively and non-invasively the accumulation of NPs in the tumor site using R2 maps.

### **3.5 *In vivo anti-tumor efficacy***

The *in vivo* anti-tumor efficacy was analyzed by following tumor volume by MRI and survival rates of the orthotopic glioma bearing mice administered NPs with different targeting strategies.

The tumor progression (Fig.4A and 4B) was analyzed by evaluating tumor volumes from ROI of MRI images obtained on day 7 and day 28 (immediately post last dose administration). On day 7, the tumor volume of all the groups was  $\sim 0.2 \text{ mm}^3$ . By day 28, the tumor progression was higher in control (saline) group with tumor volume  $\sim 3 \text{ mm}^3$ , whereas the tumor volumes in all the treated groups were in between  $1\text{-}2 \text{ mm}^3$ . The magnetic and active+magnetic groups showed the lower tumor volumes of  $\sim 1 \text{ mm}^3$ . Intra and inter tumoral heterogeneity is one of the characteristic features of GBM [40] which could evidently explain the varied degree of the therapeutic responses towards the administered NPs and the employed strategies. The acquired images showed that the tumor progression was significantly less in all the treated groups.

Fig.4C shows the survival graph of *in vivo* antitumor efficacy of PTX/SPIO-NPs and PTX/SPIO-RGD-NPs with different targeting strategies. The median survival time of control (saline) group was 38.5 days, passive targeting (PTX/SPIO-NPs) 41 days and magnetic targeting (PTX/SPIO-NPs) 46.5 days while the median survival of active targeting (PTX/SPIO-RGD-NPs) was 44 days and combination of active+magnetic targeting was 45 days. At the given doses and in the tested conditions, the magnetic targeting strategy resulted in significant survival of mice compared to control (saline) and passive targeting groups. The result is consistent with our previous report [14]. Inclusion of RGD for active targeting exerted no additional therapeutic effect when tested in combination with the magnetic strategy. However, it showed higher response than the passive and control (saline) groups.

### **3.6 *In vivo safety evaluation***

We have estimated different biochemical parameters such as AST, ALT, BUN and CKMB, to assess potential toxicity on liver, kidney and heart. The results are presented in comparison with that of Taxol (reference) (Fig. 5A). The full dosage regimen (6 doses) did not induce any significant

effect on liver, kidney and heart: there was no significant elevations of biochemical parameters observed within groups after 1 and 7 days. No significant loss in the body weights observed (supplementary data S4). From our previously reported biodistribution data, the major amounts of administered NPs were accumulated in the liver tissue. Therefore, we analyzed the liver tissue. PTX/SPIO-NPs elicited accumulation of SPIO in Kupffer cells and to lesser extent in hepatocytes after 1 and 7 days. In comparison to control (saline) group and Taxol, the tissue samples of PTX/SPIO-NPs group did not show necrosis and inflammation (Fig. 5B). The histopathological observations were corroborating the biochemical analyses indicating no significant toxicity caused by the NPs in comparison to Taxol.

#### 4. Discussion

Therapy for GBM is highly challenging, due to its aggressiveness, infiltration into surrounding normal brain tissue and recurrence. Surgical debulking of tumor is not possible in all cases. Consequently, there is need for a realistic approach of targeting GBM more selectively and less invasively by exploiting the abnormalities or differences in the permeability and vasculature of tumor in contrast to normal brain to improve the amount of drug reaching the GBM. We hypothesized that magnetic and active targeting of PTX/SPIO-NPs would enhance drug delivery to GBM and aimed to compare these different targeting strategies in an orthotopic GBM model.

We have prepared PTX/SPIO-NPs and PTX/SPIO-RGD-NPs with size ranging between 230-255 nm and with zeta potential values less than  $-15$  mV which were reported as relatively stable [41]. The encapsulation efficiency and drug loading were found to be  $\sim 30\%$  and  $\sim 1\%$  respectively. The formulations made of PLGA are usually associated with a poor drug loading [7]. Nevertheless, despite low encapsulation efficiency of PTX, our nanoformulations with PTX were able to deliver therapeutic dose of PTX (5mg/kg in 150  $\mu$ l) U87MG orthotopic nude mouse. Typically, NPs between 20-400 nm can accumulate in tumor tissues *via* EPR effect (passive targeting) [16, 17, 33, 42, 43]. Though EPR effect has been highly debated and is controversial, clinical use of various approved nanomedicines for instance, Doxil<sup>®</sup>, Abraxane<sup>®</sup> relies on EPR effect [44]. Consequently, the PTX/SPIO-NPs could benefit from the EPR effect. Hence, passive targeting was used as a baseline/ control for other targeting strategies. Even if we observed traceable amounts of NPs in the brain, passive targeting did not result in significant prolongation of survival period [14]. This could be due to the fact that insufficient quantities of NPs reach the tumor site.

SPIO in the formulation is exploited for its dual properties as superparamagnetic agent for magnetic targeting and as a  $T_2$  contrast agent for non-invasive imaging with MRI. Magnetic targeting has shown better accumulation of NPs at tumor site *via* applied external magnetic field in our *ex vivo* biodistribution study [14]. This was followed by significant inhibition of tumor progression and prolonged *in vivo* efficacy compared to passive targeting and control (saline) groups. However, magnetic targeting could result in more efficacy in regions close to the applied external magnetic field and be limited by distance between the targeted site and applied magnet, time and strength of applied magnetic field and inadequate magnetic gradients [23, 27].

Further, to explore active targeting strategy, the NPs were functionalized with RGD peptide. Grafting of RGD in the formulation specifically increased cellular uptake of NPs by TNF $\alpha$ -activated U87MG and HUVEC cells. This can be attributed to RGD affinity towards  $\alpha v \beta 3$  integrins.  $\alpha v \beta 3$  integrins were found to be over expressed on tumor cells and endothelial cells lining the tumor [45]. In addition, TNF- $\alpha$  which is present in tumor microenvironment promotes the expression of  $\alpha v \beta 3$  integrins [35, 46, 47]. However, RGD targeting did not enhance PTX cytotoxicity *in vitro* compared to untargeted NPs.

*In vitro* cytotoxicity test indicates that cytotoxic effects were mainly due to PTX. The same was true for the *in vivo* therapeutic efficacy studies. All the treated groups showed better survival than the control (saline) group. In our previous report, we analyzed PTX/SPIO-NPs efficacy using passive and magnetic targeting. The magnetic targeting resulted in significant tumor accumulation and efficacy with the dosage regimen tested [14]. In the current study, we have tested the efficacy of PTX/SPIO-NPs using active and active+magnetic targeting. From the *in vivo* efficacy results, active targeting showed a trend of improved survival compared to control (saline). Our group has reported that the active+magnetic targeting resulted in better survival of mice than the magnetic targeting in the tested CT26 subcutaneous tumor model [27]. We hypothesized that the same result of CT26 subcutaneous tumor model could also be possible in U87MG orthotopic tumor model. However, the result of U87MG orthotopic tumor model was not in full agreement with the hypothesis. Factors such as i) difference in tumor models and cell lines used ii) tumor location and barriers to drug penetration (e.g., BBB for GBM tumors) (BBB for GBM tumors) iii) size of the tumor iv)  $\alpha v \beta 3$  receptors expression on tumor endothelial cells and GBM cells might have contributed to the variant result.  $\alpha v \beta 3$  receptors play a key role in RGD targeting [48]. GBM shows heterogeneous expression of  $\alpha v \beta 3$  receptors (ranging from mild to very strong) depending on tumor

microenvironment and the rate expression of  $\alpha\beta3$  is also associated with the GBM progression [45]. We suspect that the  $\alpha\beta3$  receptors, which are needed for RGD binding, were not sufficiently either available or expressed in the tested tumor model and affected the outcome of the active targeting strategies. To fully evaluate the effects of active targeting strategies, thorough understanding of *in vivo* expression of  $\alpha\beta3$  in correlation with tumor progression is needed.

Furthermore, balancing the risks and efficacy of therapy is critical. A strategic way to achieve this balance is by tailoring a proper dosage regimen. Additionally, there is a great need to gain deep knowledge about fate of NPs *in vivo* and their associated effects at key metabolic organs. PLGA-based NPs are well known for their biocompatibility, but it is necessary to ensure that the developed PTX/SPIO-loaded PLGA nanocarriers do not exhibit major toxicological problems over multiple doses, in particular hepatotoxicity due to high accumulation in the liver [14, 49]. The dosage regimen was six injections (doses) administered every other 4th day from the first injection. The blood samples were collected 24 hours and 7 days after the last dose of administration. In our previous reports, we have evaluated the toxicity data after single intravenous injection where as in the current study we evaluated the toxicity of the full dosage regimen to better understand the overall impact of six doses. For single dose testing, a transient increase in AST levels in serum was observed which could be a general short-term response due to the hepatic accumulation of the injected NPs. On the contrary, for six dose testing, no significant changes were read for AST levels. In comparison with that of Taxol (reference), the multiple doses (6 doses) of PTX/SPIO NP did not show any significant effect on the evaluated biochemical parameters and thereby indicated that there were no major toxic effects on liver, kidney and heart.

## 5. Conclusion

The aim of the study was to evaluate different targeting strategies and their efficacy for reaching tumor site and exerting anti-tumor efficacy of PTX, a potent drug against U87GM cell (IC<sub>50</sub> 1 ng/ml). RGD grafting increased NPs uptake in activated U87MG and HUVEC cells due to favored binding to the overexpressed  $\alpha\beta3$  receptors suggesting that RGD could be a potential targeting strategy to enhance the accumulation of NPs in GBM. However, *in vivo* magnetic targeting strategy resulted in better therapeutic effect than the other groups. RGD functionalization did not exert any significant add-on effects to the magnetic targeting alone.

## Acknowledgments

We gratefully acknowledge Télévie, Belgian Fonds National de la Recherche Scientifique (FRS-FNRS) (7651916F) and Fondation contre le cancer for funding this work. We express our thanks to Kevin Vanvarenberg (Advanced Drug Delivery and Biomaterials, Université catholique de Louvain, Belgium) for his help with histology.

## Disclosure

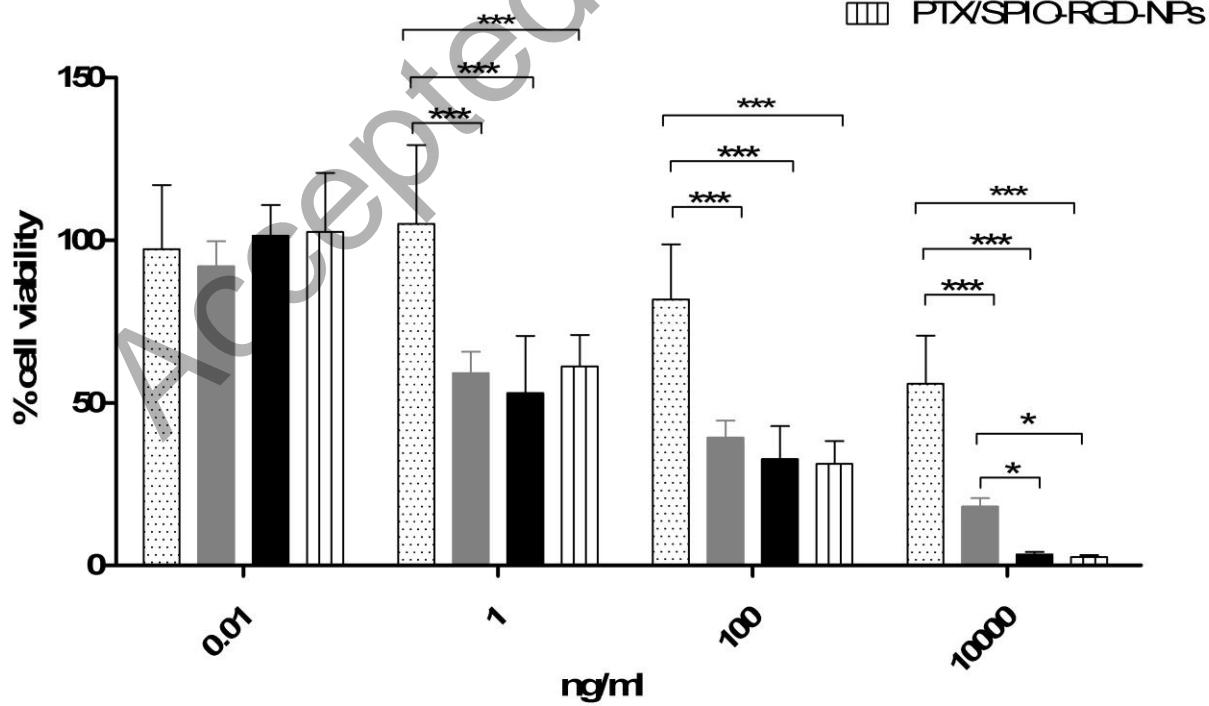
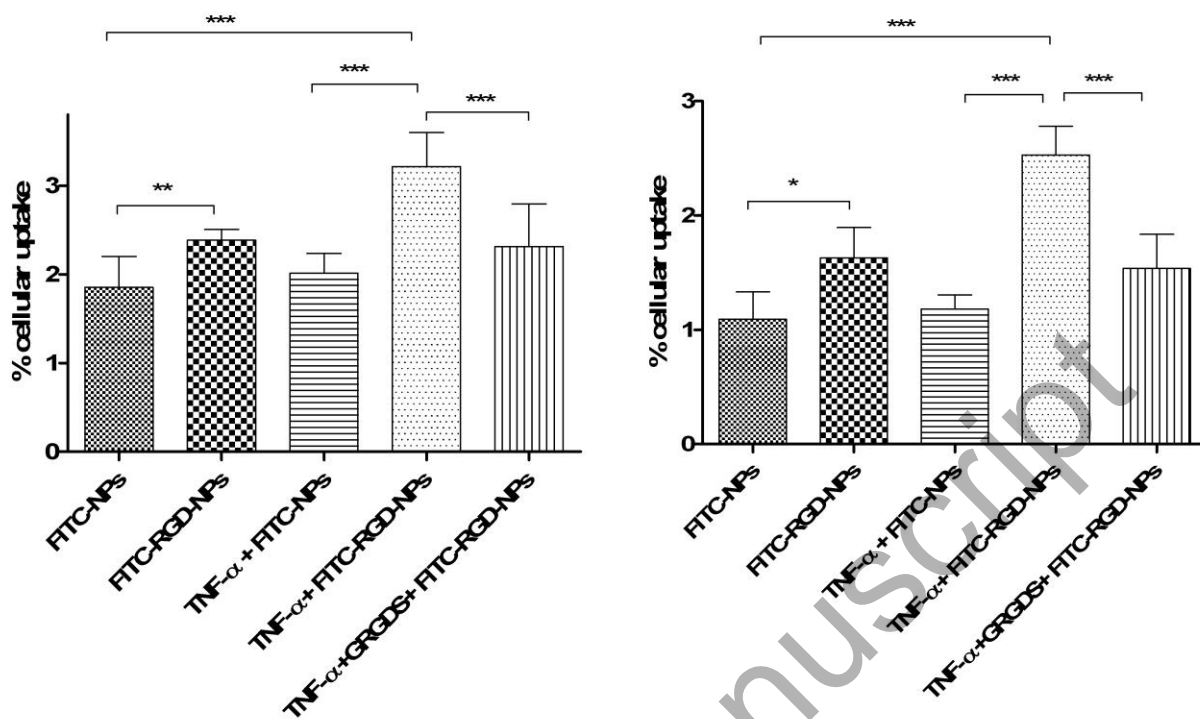
The author reports no conflicts of interest in this work.

## References

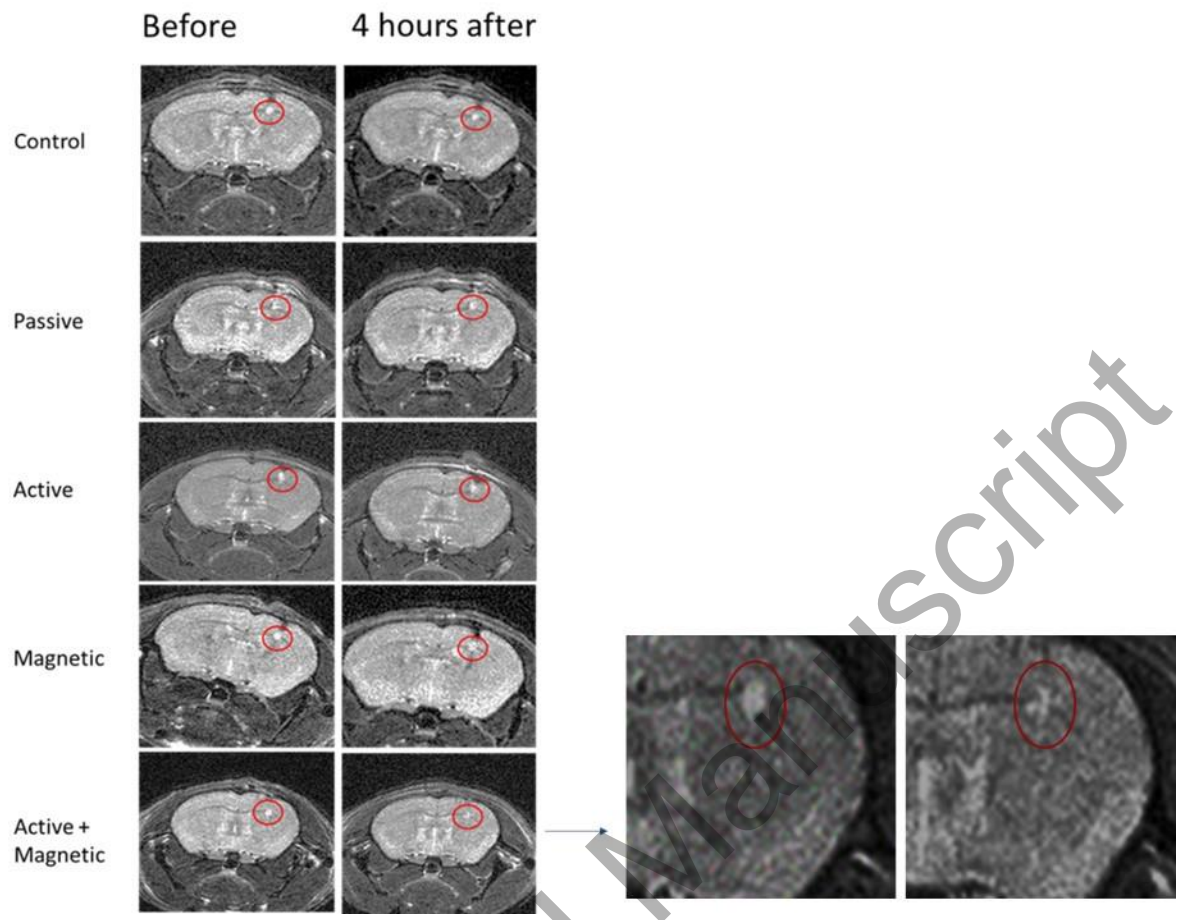
1. Stupp R, Taillibert S, Kanner AA, et al. Maintenance therapy with tumor-treating fields plus temozolomide vs temozolomide alone for glioblastoma: A randomized clinical trial. *JAMA*. 2015;314(23):2535-2543.
2. Ganipineni LP, Danhier F, Pr at V. Drug delivery challenges and future of chemotherapeutic nanomedicine for glioblastoma treatment. *J Control Release*. 2018;281:42-57.
3. Ozdemir-Kaynak E, Qutub AA, Yesil-Celiktas O. Advances in Glioblastoma Multiforme Treatment: New Models for Nanoparticle Therapy. *Front Physiol*. 2018;9:170.
4. Kang T, Zhu Q, Jiang D, et al. Synergistic targeting tenascin C and neuropilin-1 for specific penetration of nanoparticles for anti-glioblastoma treatment. *Biomaterials*. 2016;101:60-75.
5. Cho J-H, Kim AR, Kim S-H, et al. Development of a novel imaging agent using peptide-coated gold nanoparticles toward brain glioma stem cell marker CD133. *Acta Biomater*. 2017;47:182-192.
6. Jiang Y, Wang X, Liu X, et al. Enhanced Antiglioma Efficacy of Ultrahigh Loading Capacity Paclitaxel Prodrug Conjugate Self-Assembled Targeted Nanoparticles. *ACS Appl Mater Interfaces*. 2017;9(1):211-217.
7. Danhier F, Ansorena E, Silva JM, et al. PLGA-based nanoparticles: An overview of biomedical applications. *J Control Release*. 2012;161(2):505-522.
8. Strohbahn G, Coman D, Han L, et al. Imaging the delivery of brain-penetrating PLGA nanoparticles in the brain using magnetic resonance. *J Neurooncol*. 2015;121(3):441-449.
9. Arshad A, Yang B, Bienemann AS, et al. Convection-Enhanced Delivery of Carboplatin PLGA Nanoparticles for the Treatment of Glioblastoma. *PLoS One*. 2015;10(7):e0132266.
10. Weaver BA. How Taxol/paclitaxel kills cancer cells. *Mol Biol Cell*. 2014;25(18):2677-2681.
11. Wang B, Lv L, Wang Z, et al. Improved anti-glioblastoma efficacy by IL-13R $\alpha$ 2 mediated copolymer nanoparticles loaded with paclitaxel. *Sci Rep*. 2015;5:16589.
12. Liu Y, Ran R, Chen J, et al. Paclitaxel loaded liposomes decorated with a multifunctional tandem peptide for glioma targeting. *Biomaterials*. 2014;35(17):4835-4847.
13. Jiang X, Sha X, Xin H, et al. Integrin-facilitated transcytosis for enhanced penetration of advanced gliomas by poly(trimethylene carbonate)-based nanoparticles encapsulating paclitaxel. *Biomaterials*. 2013;34(12):2969-2979.

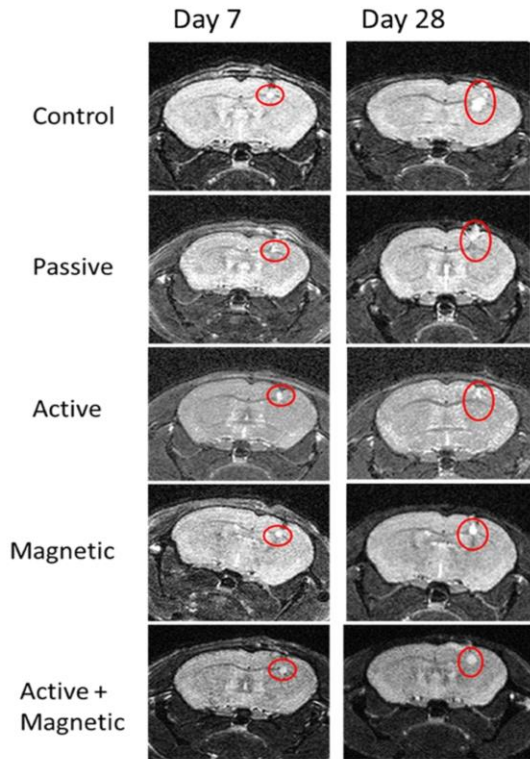
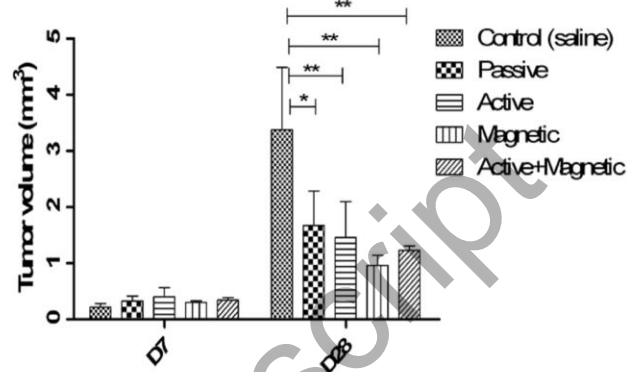
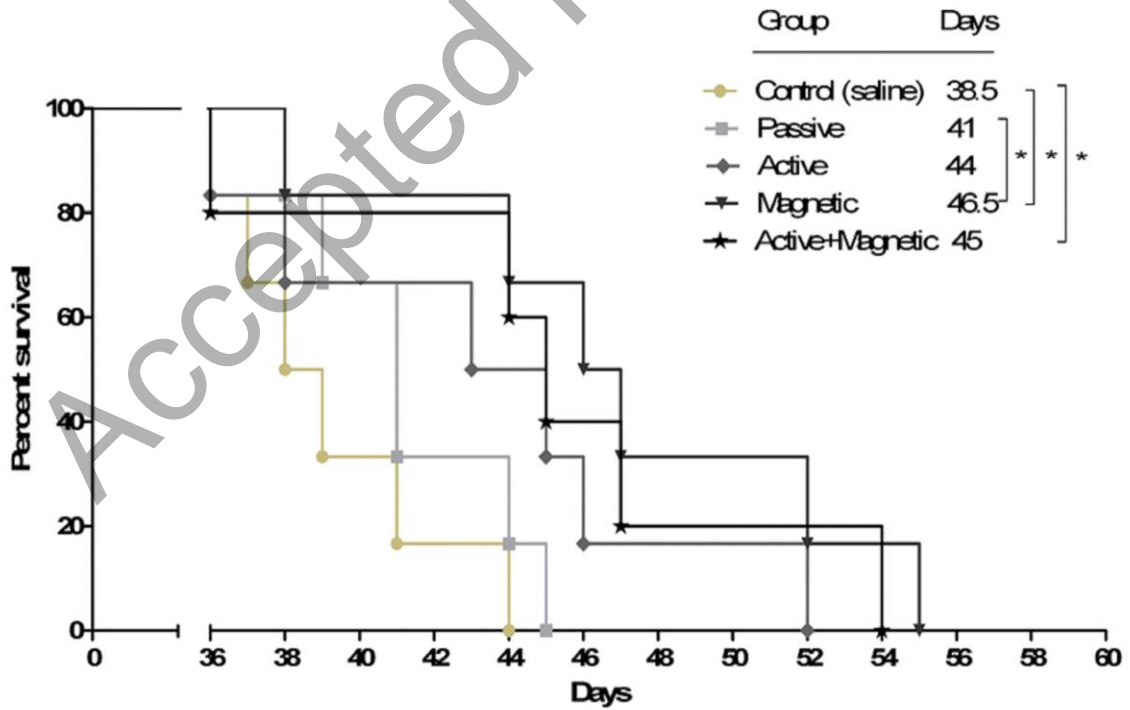
14. Ganipineni LP, Ucakar B, Joudiou N, et al. Magnetic targeting of paclitaxel-loaded poly(lactic-co-glycolic acid)-based nanoparticles for the treatment of glioblastoma. *Int J Nanomed*. 2018;13:4509-4521.
15. Zhou J, Atsina K-B, Himes BT, et al. Novel Delivery Strategies for Glioblastoma. *Cancer J*. 2012;18(1):89-99.
16. Danhier F, Feron O, Pr at V. To exploit the tumor microenvironment: Passive and active tumor targeting of nanocarriers for anti-cancer drug delivery. *J Control Release*. 2010;148(2):135-146.
17. Danhier F. To exploit the tumor microenvironment: Since the EPR effect fails in the clinic, what is the future of nanomedicine? *J Control Release*. 2016;244:108-121.
18. D'Abaco GM, Kaye AH. Integrins: Molecular determinants of glioma invasion. *J Clin Neurosci*. 2007;14(11):1041-1048.
19. Franovic A, Elliott KC, Seguin L, et al. Glioblastomas require integrin  $\alpha\beta3$ /PAK4 signaling to escape senescence. *Cancer Res*. 2015;75(21):4466-4473.
20. Ye Y, Xu B, Nikiforovich GV, et al. Exploring new near-infrared fluorescent disulfide-based cyclic RGD peptide analogs for potential integrin-targeted optical imaging. *Bioorg Med Chem Lett*. 2011;21(7):2116-2120.
21. Danhier F, Le Breton A, Pr at V. RGD-Based Strategies To Target Alpha(v) Beta(3) Integrin in Cancer Therapy and Diagnosis. *Mol Pharm*. 2012;9(11):2961-2973.
22. Polyak B, Friedman G. Magnetic targeting for site-specific drug delivery: applications and clinical potential. *Expert Opin on Drug Deliv*. 2009;6(1):53-70.
23. Chertok B, Moffat BA, David AE, et al. Iron Oxide Nanoparticles as a Drug Delivery Vehicle for MRI Monitored Magnetic Targeting of Brain Tumors. *Biomaterials*. 2008;29(4):487-496.
24. Fontes de Paula Aguiar M, Bustamante Mamani J, Klei Felix T, et al. Magnetic targeting with superparamagnetic iron oxide nanoparticles for in vivo glioma. *Nanotechnology Reviews* 2017. p. 449.
25. Lee C, Kim GR, Yoon J, et al. In vivo delineation of glioblastoma by targeting tumor-associated macrophages with near-infrared fluorescent silica coated iron oxide nanoparticles in orthotopic xenografts for surgical guidance. *Sci Rep*. 2018;8(1):11122.
26. Wankhede M, Bouras A, Kaluzova M, et al. Magnetic nanoparticles: an emerging technology for malignant brain tumor imaging and therapy. *Expert Rev Clin Pharmacol*. 2012;5(2):173-186.
27. Schleich N, Po C, Jacobs D, et al. Comparison of active, passive and magnetic targeting to tumors of multifunctional paclitaxel/SPIO-loaded nanoparticles for tumor imaging and therapy. *J Control Release*. 2014;194:82-91.
28. Pourcelle V, Freichels H, Stoffelbach F, et al. Light Induced Functionalization of PCL-PEG Block Copolymers for the Covalent Immobilization of Biomolecules. *Biomacromolecules*. 2009;10(4):966-974.
29. Freichels H, Danhier F, Pr at V, et al. Fluorescent Labeling of Degradable Poly(Lactide-Co-Glycolide) for Cellular Nanoparticles Tracking in Living Cells. *Int J Artif Organs*. 2011;34(2):152-160.
30. Garinot M, Fi vez V, Pourcelle V, et al. PEGylated PLGA-based nanoparticles targeting M cells for oral vaccination. *J Control Release*. 2007;120(3):195-204.

31. Pourcelle V, Devouge S, Garinot M, et al. PCL-PEG-Based Nanoparticles Grafted with GRGDS Peptide: Preparation and Surface Analysis by XPS. *Biomacromolecules*. 2007;8(12):3977-3983.
32. Massart R. Preparation of aqueous magnetic liquids in alkaline and acidic media. *IEEE T on MAGN*. 1981;17(2):1247-1248.
33. Schleich N, Sibret P, Danhier P, et al. Dual anticancer drug/superparamagnetic iron oxide-loaded PLGA-based nanoparticles for cancer therapy and magnetic resonance imaging. *Int J Pharm*. 2013;447(1):94-101.
34. Chang M-W, Lo J-M, Juan H-F, et al. Combination of RGD Compound and Low-Dose Paclitaxel Induces Apoptosis in Human Glioblastoma Cells. *PLoS One*. 2012;7(5):e37935.
35. Danhier F, Vroman B, Lecouturier N, et al. Targeting of tumor endothelium by RGD-grafted PLGA-nanoparticles loaded with Paclitaxel. *J Control Release*. 2009;140(2):166-173.
36. Bastiancich C, Vanvarenberg K, Ucar B, et al. Lauroyl-gemcitabine-loaded lipid nanocapsule hydrogel for the treatment of glioblastoma. *J Control Release*. 2016;225:283-293.
37. Cui Y, Zhang M, Zeng F, et al. Dual-Targeting Magnetic PLGA Nanoparticles for Codelivery of Paclitaxel and Curcumin for Brain Tumor Therapy. *ACS Appl Mater Interfaces*. 2016;8(47):32159-32169.
38. Gu G, Hu Q, Feng X, et al. PEG-PLA nanoparticles modified with APTEDB peptide for enhanced anti-angiogenic and anti-glioma therapy. *Biomaterials*. 2014;35(28):8215-8226.
39. Kang W, Svirskis D, Sarojini V, et al. Cyclic-RGDyC functionalized liposomes for dual-targeting of tumor vasculature and cancer cells in glioblastoma: An in vitro boron neutron capture therapy study. *Oncotarget*. 2017;8(22):36614-36627.
40. Inda M-d-M, Bonavia R, Seoane J. Glioblastoma Multiforme: A Look Inside Its Heterogeneous Nature. *Cancers (Basel)*. 2014;6(1):226-239.
41. Bhattacharjee S. DLS and zeta potential – What they are and what they are not? *J Control Release*. 2016;235:337-351.
42. Maeda H, Wu J, Sawa T, et al. Tumor vascular permeability and the EPR effect in macromolecular therapeutics: a review. *J Control Release*. 2000;65(1):271-284.
43. Lammers T, Kiessling F, Hennink WE, et al. Drug targeting to tumors: Principles, pitfalls and (pre-) clinical progress. *J Control Release*. 2012;161(2):175-187.
44. Rosenblum D, Joshi N, Tao W, et al. Progress and challenges towards targeted delivery of cancer therapeutics. *Nat Commun*. 2018;9(1):1410.
45. Schnell O, Krebs B, Wagner E, et al. Expression of Integrin  $\alpha(v)\beta(3)$  in Gliomas Correlates with Tumor Grade and Is not Restricted to Tumor Vasculature. *Brain Pathol*. 2008;18(3):378-386.
46. Hou C-H, Yang R-S, Hou S-M, et al. TNF- $\alpha$  increases  $\alpha v \beta 3$  integrin expression and migration in human chondrosarcoma cells. *J Cell Physiol*. 2010;226(3):792-799.
47. Brüning A, Runnebaum IB. CAR is a cell-cell adhesion protein in human cancer cells and is expressionally modulated by dexamethasone, TNF $\alpha$ , and TGF $\beta$ . *Gene Ther*. 2003;10:198.
48. Wang F, Li Y, Shen Y, et al. The functions and applications of RGD in tumor therapy and tissue engineering. *Int J Mol Sci*. 2013;14(7):13447-13462.
49. Blanco E, Shen H, Ferrari M. Principles of nanoparticle design for overcoming biological barriers to drug delivery. *Nat Biotechnol*. 2015;33(9):941-951.



SPION-NPs  
 PTX-NPs  
 PTX/SPION-NPs  
 PTX/SPION-RGD-NPs



**A****B****C**

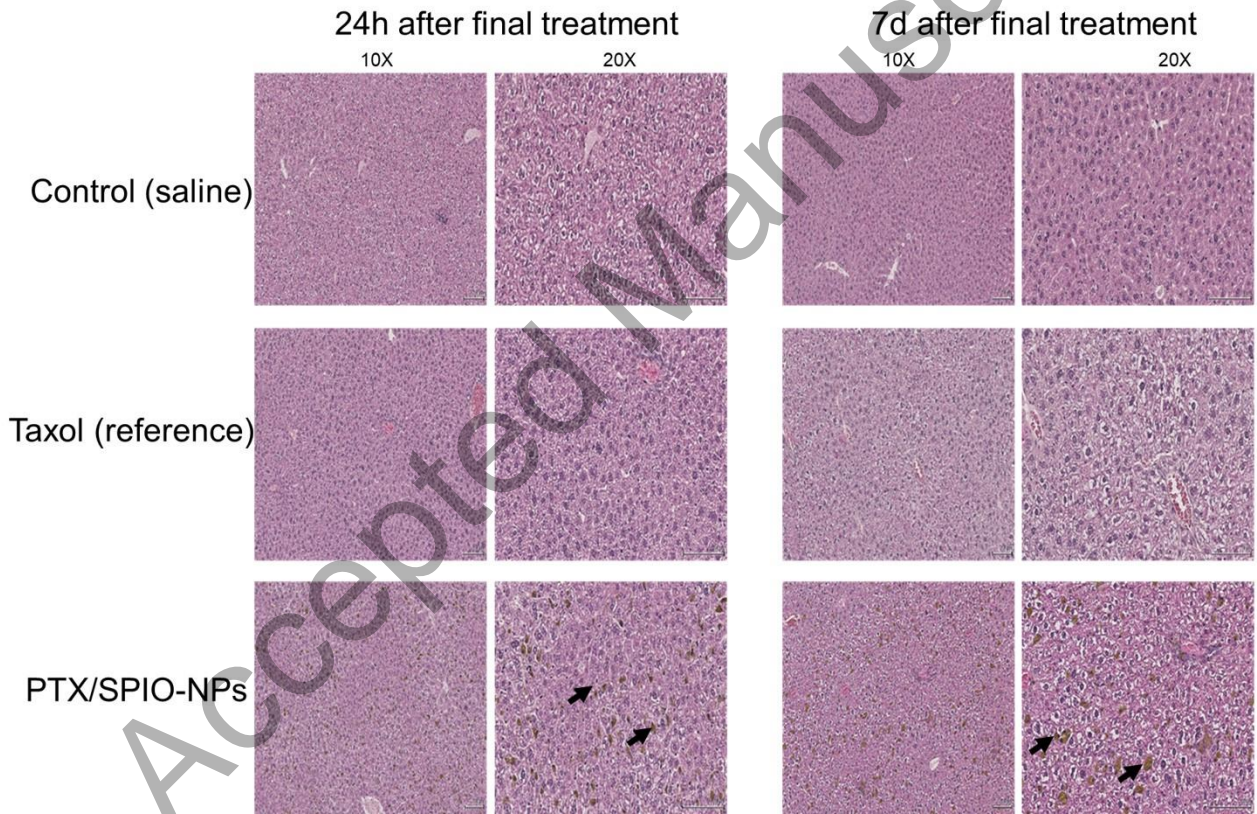
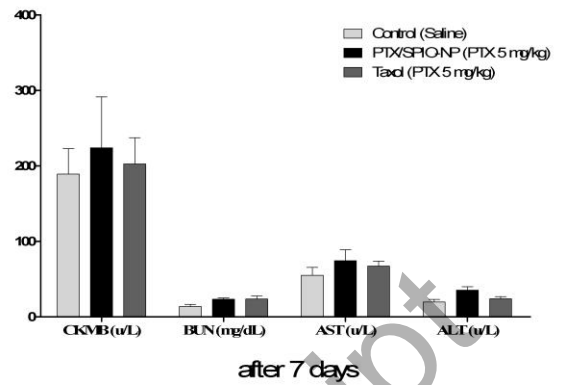
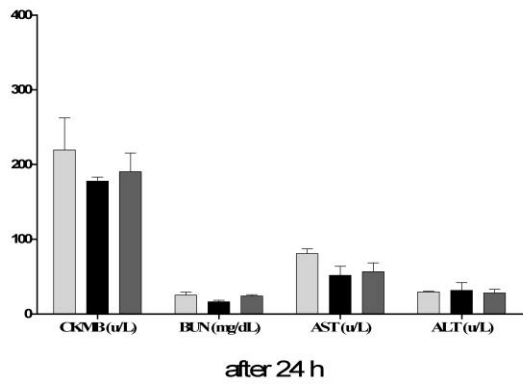


Table 1: Physicochemical characterization of various NPs FITC-NPs, FITC RGD-NPs, SPIO-NPs, PTX-NPs, PTX/SPIO-NPs and PTX/SPIO-RGD-NPs (n ≥ 3).

	<b>FITC - NPs</b>	<b>FITC RGD - NPs</b>	<b>SPIO-NPs</b>	<b>PTX-NPs</b>	<b>PTX/SPIO-NPs</b>	<b>PTX/SPIO-RGD-NPs</b>
Size (nm)	220 ± 8	229 ± 10	230 ± 5	224 ± 12	247 ± 10	255 ± 15
PDI	0.14	0.18	0.15	0.11	0.17	0.15
zeta potential (mV)	-16 ± 2	-18 ± 4	-14 ± 3	-22 ± 5	-17 ± 7	-19 ± 7
Drug encapsulation efficiency (%)	NA	NA	NA	29 ± 3	31 ± 5	27 ± 5
Drug loading (%)	NA	NA	NA	0.88 ± 0.4	0.83 ± 0.5	0.80 ± 0.3
Iron loading (%)	NA	NA	3 ± 1	NA	3.5 ± 0.5	3 ± 1